Orientation Relations During the α-ω Phase Transition of Zirconium: *In Situ* Texture Observations at High Pressure and Temperature

H.-R. Wenk,[1,*] P. Kaercher,[1] W. Kanitpanyacharoen,[1] E. Zepeda-Alarcon,[1] and Y. Wang[2]
[1]*Department of Earth and Planetary Science, University of California, Berkeley, California 94720, USA*
[2]*Center for Advanced Radiation Sources, The University of Chicago, Chicago, Illinois 60637, USA*
(Received 15 May 2013; published 6 November 2013)

Transition metals Ti, Zr, and Hf have a hexagonal close-packed structure (α) at ambient conditions, but undergo phase transformations with increasing temperature and pressure. Of particular significance is the high-pressure hexagonal ω phase which is brittle compared to the α phase. There has been a long debate about transformation mechanisms and orientation relations between the two crystal structures. Here we present the first high pressure experiments with *in situ* synchrotron x-ray diffraction texture studies on polycrystalline aggregates. We follow crystal orientation changes in Zr, confirming the original suggestion by Silcock for an $\alpha \rightarrow \omega$ martensitic transition for Ti, with $(0001)_\alpha || (11\bar{2}0)_\omega$, and a remarkable orientation memory when ω reverts back to α.

DOI: 10.1103/PhysRevLett.111.195701 PACS numbers: 64.70.kd, 07.85.Qe, 62.50.−p

At ambient conditions transition metals such as titanium, zirconium, and hafnium crystallize in a distorted hexagonal close-packed structure (α). These metals have received a great deal of attention, particularly due to the importance of Ti as a light structural metal, and Zr and Hf as components of nuclear reactors. At high temperature the α phase of these metals transforms to a body-centered-cubic (bcc) structure (β), while at high pressure it converts to a different hexagonal structure (ω) (Fig. 1). The $\alpha \rightarrow \omega$ transition is significant from a mechanistic point of view, since the α phase is ductile and the ω phase is brittle. The ω phase was first discovered in Ti alloys that were quenched from the high temperature β structure [1]. Later, static high pressure experiments established that the ω structure is stable at high pressure [2–5], which was further confirmed by shock experiments [6]. In all previous experiments the ω phase did not revert to the α phase at pressure release and was analyzed at ambient conditions. The phase relations of Zr have been studied experimentally and equations of state were established [7,8].

The electronic transfer between the broad sp band and the much narrower d band in group IV transition metals is a likely driving force behind structural transitions [9] and has stimulated a large number of molecular dynamic investigations that explore the changes in bonding [10–13].

The hexagonal ω structure has been described as a distorted bcc structure [14,15] which can be achieved by displacing atoms in the α structure (Fig. 1). Orientation relationships between α and ω were explored with x-ray diffraction [1], transmission electron microscopy [16,17], and *ab initio* calculations [18] to investigate the martensitic nature of the transformation. While orientation changes and texture memory in the $\alpha \rightarrow \beta$ phase transition in Ti have been extensively studied *in situ* [19], and a martensitic mechanism described by Burgers [20] is firmly established with the topotactic relations $(0001)_\alpha || \{110\}_\beta$, i.e., the (0001) plane in α becomes equivalent to the {110} planes in β, and $\langle 11\bar{2}0\rangle_\alpha || \langle 1\bar{1}1\rangle_\beta$, there is still considerable debate about the martensitic mechanism during the $\alpha \rightarrow \omega$ transformation. For Ti the mechanism originally suggested by Silcock [1] with $(0001)_\alpha || (11\bar{2}0)_\omega$ and $[11\bar{2}0]_\alpha || [0001]_\omega$ is at odds with the *ab initio* calculations

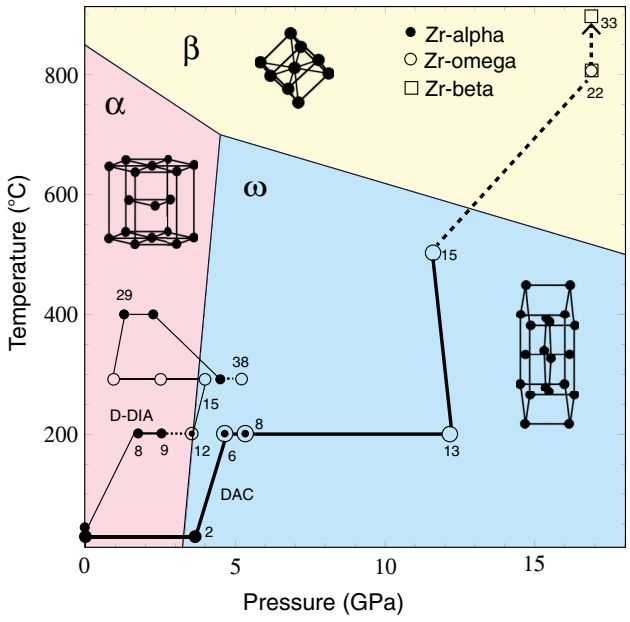

FIG. 1 (color online). The pressure-temperature paths for D-DIA and DAC experiments are shown within the Zhang *et al.* [27] phase diagram. Dotted lines in D-DIA experiments indicate large compressive strain. Dashed lines in DAC experiments indicate uncertainties in pressure estimates for the ω phase at higher temperature. The structures of the three phases are illustrated in assumed orientations and on the same scale. Numbers refer to diffraction images in Table I.

of electronic structures by Trinkle *et al.* [18] where $(0001)_\alpha||(01\bar{1}1)_\omega$ and $[11\bar{2}0]_\alpha||[01\bar{1}1]_\omega$.

While previous investigations relied on observations of orientation relations in single crystals and modeling of bonding energies, here we apply high pressure and temperature diffraction experiments on polycrystals to explore *in situ* crystallographic orientation development and changes during the $\alpha \rightarrow \omega$ and $\omega \rightarrow \alpha$ phase transitions in Zr. This work is an extension of previous experiments on hcp metals to determine the role of pressure on deformation mechanisms [21], including ε-iron (hcp) [22].

The first set of experiments was conducted with a multi anvil apparatus, the Deformation-DIA (D-DIA) at beam line 13-BM-D of the Advanced Photon Source, which allows for relatively large samples and flexibility in controlling the loading history [23]. The D-DIA consists of three pairs of tungsten carbide anvils, one of which can be controlled independently, enabling users to change differential stress independent of quasi-hydrostatic pressure. Cylindrical samples of high purity (99.9%) Zr wire, obtained from ESPI Metals (K5957j), 0.5 mm in diameter, were cut to 0.8 mm length. The sample was loaded into a cubic boron-nitride sleeve, capped with alumina pistons, and set inside of a cylindrical graphite heater in a cubic pressure medium made of a mixture of amorphous boron and epoxy (BE). Pyrophyllite gaskets at the edges of the BE cube were used to maintain alignment of the BE cube in the x-ray beam, and their peaks also appear in diffraction patterns. An x-ray beam of wavelength 0.20663 Å was collimated to 200×200 μm. Diffraction images were recorded on a Mar165 charge-coupled device for 300 sec. This detector was binned to 2048×2048 pixels with a pixel size of 0.079 mm. In addition, x-ray radiography recorded the changes of wire length, providing a direct measure of macroscopic axial strain (ε), defined as $\varepsilon(\%) = 100 \times (1 - l/l_0)$, where l_0 is the initial sample length after quasi-hydrostatic compression.

The second experiment was done with a diamond anvil cell (DAC) in radial diffraction geometry at beam line 12.2.2 of the Advanced Light Source [24]. A monochromatic x-ray beam with wavelength 0.49594 Å was focused to 20×20 μm and used to penetrate through an x-ray transparent boron-kapton gasket and the same polycrystalline sample of Zr. Without inserting a pressure medium, diamond anvils impose a differential compressive stress in addition to hydrostatic pressure, causing crystals to reorient. Diffraction images were recorded with a Mar345 image plate detector binned to 3450×3450 pixels with a pixel size of 0.1 mm. The DAC experiments cannot reverse strain but can achieve much higher pressures and temperatures. Temperature was increased by combined resistive and laser heating [25]. Axial plastic strain is difficult to estimate for DAC experiments due to the small sample size, the effect of the confining gasket material, compaction of the original sample, and the geometry of the DAC and gasket. According to studies of texture development in previous DAC experiments, it is estimated that axial strain of 20%–25% may be reached at 20 GPa [21,24].

Diffraction data from both experiments were analyzed by the Rietveld method implemented in the software MAUD [26], which uses a least-squares approach to minimize the difference between experimental diffraction data and a calculated model based on crystal structure and microstructural characteristics. Figure 2(a) displays stacks of experimental diffraction patterns for Zr at different conditions for the D-DIA experiments and Fig. 2(b) shows corresponding patterns for the DAC experiments. The variation of intensity with azimuth (vertical axis) immediately reveals crystallographic preferred orientation. Sinusoidal variations in peak positions result from elastic distortion of lattice planes due to deviatoric stress imposed by the D-DIA or DAC on the sample. The pressure was determined by fitting unit cell parameters of Zr with a third-order Birch-Murnaghan equation of state (Table I). Values for bulk modulus (K_0) and pressure and temperature derivatives for α Zr were taken from Zhao *et al.* [7]. Uncertainties are estimated to be 0.2–1 GPa with higher values for high pressures. Details of the experiments are summarized in Table I, and experimental paths in pressure-temperature space are shown in Fig. 1.

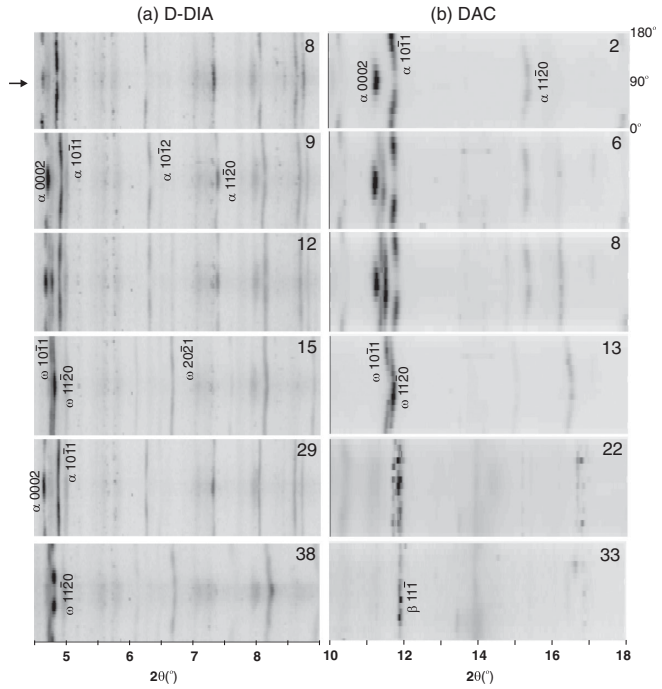

FIG. 2. Measured diffraction spectra as a function of 2θ for the 0°–180° azimuthal sector of the image. Compression direction is marked with an arrow. Some α and ω diffraction peaks are labeled. Numbers in the upper right corner of each pattern refer to recorded images in Table I. (a) D-DIA, (b) DAC.

TABLE I. Summary of experimental conditions and results. Strain refers to standard strain, $\varepsilon(\%) = 100 \times (1 - l/l_0)$.

Image #	Phase	Volume fraction	P (GPa)	T (°C)	Strain (%)	Max pole density (m.r.d.)
D-DIA						
3	α	1	0	25	0	3.6
8[a]	α	1	1.8	200	7	3.4
9[a]	α	1	2.7	200	13	6.4
10	α	0.90	2.8	200	18	7.0
	ω	0.10				5.2
11	α	0.77	3.0	200	19	5.5
	ω	0.23				3.5
12[a]	α	0.56	3.3	200	19	6.0
	ω	0.44				4.6
13	α	0.55	3.4	300	19	4.7
	ω	0.45				3.9
14	α	0.14	4.6	300	19	5.4
	ω	0.86				3.5
15[a]	ω	1	4.5	300	19	3.0
16	ω	1	2.1	300	24	2.6
25	ω	1	0.4	300	23	2.5
28	α	1	1.1	400	21	4.8
29[a]	α	1	1.2	400	20	4.9
31	α	1	2.2	400	20	4.0
34	α	1	3.6	300	21	3.1
35	ω	1	5.2	300	30	2.7
38[a]	ω	1	4.9	300	50	6.8
DAC						
1	α	1	0.0	25		-
2[b]	α	1	3.8	25		7.7
6[b]	α	0.2	4.2	200		7.2
	ω	0.8				1.6
8[b]	α	0.23	5.2	200		7.3
	ω	0.77				1.4
13[b]	ω	1	12.2	200		2.1
15	ω	1	11.6	500		1.2
22[b]	ω	0.68	~15	800		-
	β	0.32				-
33[b]	β	1	~15	1500		-

[a]Shown in Fig. 2(a).
[b]Shown in Fig. 2(b).

Orientation distribution functions were computed in MAUD based on intensity variations in Debye rings (Fig. 2). For both D-DIA and DAC experiments, we imposed axial strain and thus expect axial symmetry of the texture pattern. Inverse pole figures (IPFs), which describe the orientation of the compression axis relative to the crystal coordinates [labeled in Fig. 3(a)-8], are used for representation. Because of the hexagonal crystal symmetry, a 30° partial IPF is sufficient to represent complete texture information. Pole densities are expressed as multiples of a random distribution (m.r.d.), where 1 m.r.d. corresponds to no preferred orientation. IPFs for D-DIA and DAC experiments are displayed in Fig. 3.

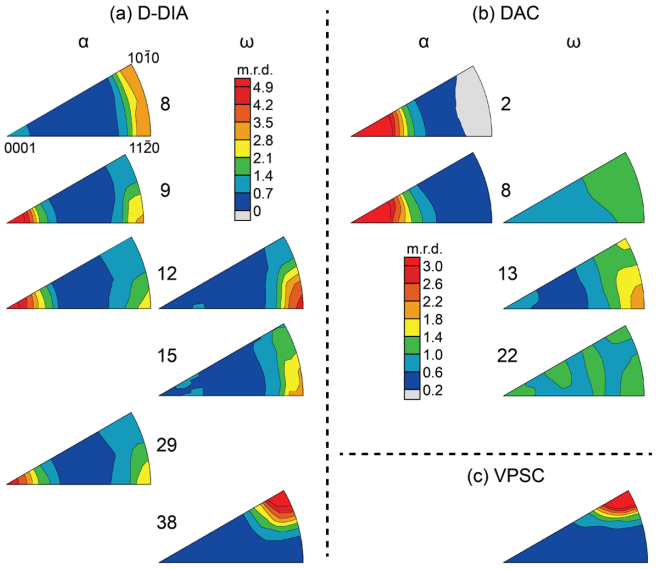

FIG. 3 (color online). Selected inverse pole figures. Equal area projection, contours in multiples of a random distribution (m.r.d.). (a) D-DIA, (08) initial wire texture, (09) after compression the texture changes due to tensile twinning and basal slip, (12) α and ω coexist with strong textures, (15) ω texture after phase transition, (29) perfect texture memory after ω reverts back to α, (38) compression of ω to 50% strain produces a deformation texture. (b) DAC. (02) α compression texture, (08) α partially converting to ω, (13) fully transformed to ω, (22) grain growth during recrystallization at high temperature. (c) VPSC model. Pattern (38) in (a) can be explained by polycrystal plasticity as dominant prismatic and basal slips on $\{11\bar{2}0\}\langle 10\bar{1}0\rangle$ and $(0001)\langle 10\bar{1}0\rangle$.

In D-DIA experiments the initial α Zr wire sample showed a typical hcp wire texture with maxima centered at $11\bar{2}0$ and $10\bar{1}0$ [Fig. 3(a)-8]. After compression to 2.5 GPa at 200 °C and shortening to 13% strain, the maximum pole distribution shifted to 0001 [Fig. 3(a)-9], mainly due to tensile twinning and basal slip [21]. With further pressure increase to 3 GPa the ω phase started to nucleate [Fig. 2(a)-12], with a maximum at $11\bar{2}0$ in the IPF [Fig. 3(a)-12]. The metastable α phase gradually disappeared, especially after increasing temperature to 300 °C [Fig. 2(a)-15]. Pressure was then reduced to 1.1 GPa, maintaining the ω phase without significant changes in phase or texture. At that point temperature was increased to 400 °C, inducing a reversion of the metastable ω phase to the stable α phase [Fig. 2(a)-29] with an α texture identical to the previous α texture [i.e., a main maximum at 0001 and a subsidiary maximum at $11\bar{2}0$, Fig. 3(a)-9 versus 3(a)-29]. This phenomenon documents a perfect memory after cycling through the ω phase. The temperature was then reduced again to 300 °C and pressure increased to 4.5 GPa to return to the ω phase. Next the sample was strained to 50% in compression, inducing a

strong ω texture with a maximum in the IPF at $10\bar{1}0$ [Fig. 3(a)-38].

Analogous changes were observed in DAC experiments. To account for kinetic barriers during the phase transition, resistive heating to 200 °C was applied [25]. A strong texture with a 0001 maximum in the IPF, similar to the D-DIA experiment [Fig. 3(a)-9], developed at 3 GPa [Fig. 2(b)-2 and Fig. 3(b)-2]. At 5 GPa the ω phase started to evolve and coexisted with a metastable α phase [Fig. 2(b)-6 and 8]. At higher pressure (~12 GPa), only ω was present [Fig. 2(b)-13] and had a maximum at $11\bar{2}0$ in the IPF [Fig. 3(b)-13], just as in the D-DIA experiments. Temperature was then increased, first by resistive heating up to 800 °C, and later combined with laser heating to 1500 °C [25]. There was considerable grain growth, and the pattern became spotty with no clear preferred orientation [Fig. 2(b)-22]. In the DAC experiments at higher temperature, stresses and strain are minimal and textures became randomized. Ultimately the material transformed to β [Fig. 2(b)-33] but with no clear texture pattern due to coarse grain size.

Contrary to earlier studies that relied on single crystal x-ray [1], electron microscopy of recovered ω crystals [16], and first principle predictions based on bonding energies [18], our investigation is the first analysis to explore the orientation relations of aggregates *in situ* during pressure and temperature changes. Also, we use Zr rather than Ti on which most previous work was done. The IPFs document a strong orientation relationship between the parent α texture [Fig. 3(a)-12 for D-DIA and Fig. 3(b)-8 for DAC] and the subsequent ω texture [Fig. 3(a)-12 for D-DIA and Fig. 3(b)-8 for DAC]. Furthermore, D-DIA experiments show a perfect texture memory for the α phase which has been cycled through the ω phase, even reproducing the subsidiary maximum at $11\bar{2}0$ [Fig. 3(a)-29]. This suggests a purely martensitic phase transition. Because of kinetic barriers the phase transitions could only be observed *in situ* at moderate temperatures, at least within the explored pressure range. Based on the D-DIA and DAC experiments, it appears that the transition occurs at ~200 °C at 3.5 GPa, consistent with the phase diagram [27].

Orientation relations are best visible in pole figures (Fig. 4). It is apparent that Silcock's [1] suggestion of $(0001)_\alpha||(11\bar{2}0)_\omega$ for Ti applies to the texture patterns of Zr in our experiments. Silcock's second condition $[11\bar{2}0]_\alpha||[0001]_\omega$ is more difficult to establish with a fiber texture and an initial (0001) maximum in the fiber direction. Pole figures are not congruent with this relation, but rather a $[10\bar{1}0]_\alpha||[0001]_\omega$ relationship. This aspect should be further studied with different starting textures. The texture memory implies that the same relationship applies for the reverse transition. In the phase diagram (Fig. 1) the different structures are plotted relative to α using the Burgers relation [20] for β and the Silcock relation [1]

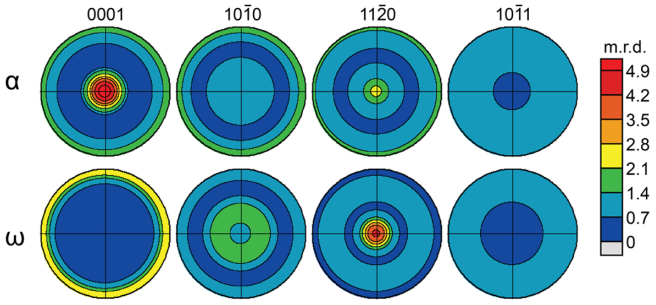

FIG. 4 (color online). Selected pole figures for D-DIA diffraction pattern #12 where the two phases coexist. Compression direction is in center of pole figures. They clearly demonstrate a $(0001)\alpha \leftrightarrow (11\bar{2}0)\omega$ correspondence. Equal area projection.

for ω. Close structural similarities can be recognized which have been discussed previously [16]. The observed $(0001)_\alpha||(11\bar{2}0)_\omega$ correspondence in Zr does not exclude that different relationships may exist for Ti and Ti alloys proposed on the basis of bonding-energy considerations [11], though there is no experimental evidence.

Further deformation of the ω phase at 5 GPa and 300 °C to 50% axial shortening with the D-DIA changes the orientation pattern, with the IPF maximum shifting to $(10\bar{1}0)$ [Fig. 3(a)-38] due to slip systems being activated by the increased strain. Plausible deformation mechanisms can be obtained by comparing experiments with polycrystal plasticity simulations. Using the Los Alamos viscoplastic self-consistent model (VPSC) [28], trying different combinations of slip systems and changing their activities, we find that a combination of prismatic slip $\{11\bar{2}0\}\langle 10\bar{1}0\rangle$, i.e., dislocations in the $\{11\bar{2}0\}$ crystallographic planes propagate in the $\langle 10\bar{1}0\rangle$ direction, combined with basal slip $(0001)\langle 10\bar{1}0\rangle$ best explains how lattice planes rotate to produce the observed texture pattern [Fig. 3(c)-VPSC].

Methods developed in mineral physics for high pressure deformation experiments and data analysis shed new light on phase transitions and deformation mechanisms of transition metals. In the future similar methods should be used to investigate different starting textures of Zr, Ti, and Hf and experimentally explore the potential influence of composition and impurity content.

This project was supported by grants from CDAC and NSF EAR 0836402 and EAR 0968456. We appreciate the access to beam lines 12.2.2 at the Advanced Light Source and 13-BM-D at the Advanced Photon Source to conduct high pressure experiments. GeoSoilEnviroCARS is supported by the National Science Foundation - Earth Sciences (EAR-1128799) and Department of Energy - Geosciences (DE-FG02-94ER14466). Use of the Advanced Light Source and the Advanced Photon Source was supported by the U.S. Department of Energy, Office of Basic Energy Sciences, under Contracts No. DE-AC02-05CH11231 and DE-AC02-06CH11357, respectively.

*wenk@berkeley.edu

[1] J. M. Silcock, Acta Metall. **6**, 481 (1958).
[2] J. C. Jamieson, Science **140**, 72 (1963).
[3] A. Jayaraman, J. W. Klement, and G. C. Kennedy, Phys. Rev. **131**, 644 (1963).
[4] Y. K Vohra, S. K. Sikka, S. N. Vaidya, and R. Chidambaram, J. Phys. Chem. Solids **38**, 1293 (1977).
[5] V. A. Zilbershteyn, N. P. Chistotina, A. A. Zharov, N. S. Grishina, and E. I. Estrin, Fiz. Met. Metalloved. **39**, 445 (1975).
[6] C. W. Greeff, D. R. Trinkle, and R. C. Albers, J. Appl. Phys. **90**, 2221 (2001).
[7] Y. Zhao *et al.*, Phys. Rev. B **71**, 184119 (2005).
[8] Y. Zhao and J. Zhang, Appl. Phys. Lett. **91**, 201907 (2007).
[9] Y. K. Vohra, Acta Metall. **27**, 1671 (1979).
[10] S. A. Ostanin and V. Y. Trubitsin, Phys. Rev. B **57**, 13 485 (1998).
[11] R. G. Hennig, D. R. Trinkle, J. Bouchet, S. G. Srivastava, R. C. Albers, and J. W. Wilkins, Nat. Mater. **4**, 129 (2005).
[12] I. Schnell and R. C. Albers, J. Phys. Condens. Matter **18**, 1483 (2006).
[13] Y. J. Hao, L. Zhang, X. R. Chen, L. C. Cai, Q. Wu, and D. Alfè, Phys. Rev. B **78**, 134101 (2008).
[14] D. DeFontaine, Acta Metall. **18**, 275 (1970).
[15] R. Pynn, J. Phys. F **8**, 1 (1978).
[16] A. Rabinkin, M. Talianker, and O. Botstein, Acta Metall. **29**, 691 (1981).
[17] G. A. Sargent and H. Conrad, Mater. Sci. Eng. **7**, 220 (1971).
[18] D. R. Trinkle, R. G. Hennig, S. G. Srinivasan, D. M. Hatch, M. D. Jones, H. T. Stokes, R. C. Albers and J. W. Wilkins, Phys. Rev. Lett. **91**, 025701 (2003).
[19] I. Lonardelli, N. Gey, H.-R. Wenk, M. Humbert, S. C. Vogel, and L. Lutterotti, Acta Mater. **55**, 5718 (2007).
[20] W. G. Burgers, Physica (Amsterdam) **1**, 561 (1934).
[21] W. Kanitpanyacharoen, S. Merkel, L. Miyagi, P. Kaercher, C. Tome, Y. Wang, and H.-R. Wenk, Acta Mater. **60**, 430 (2012).
[22] S. Merkel, H. P. Liermann, L. Miyagi, and H.-R. Wenk, Acta Mater. **61**, 5144 (2013).
[23] Y. Wang, W. B. Durham, I. C. Getting, and D. J. Weidner, Rev. Sci. Instrum. **74**, 3002 (2003).
[24] L. Miyagi, W. Kanitpanyacharoen, P. Kaercher, K. K. M. Lee, and H. R. Wenk, Science **329**, 1639 (2010).
[25] L. Miyagi, W. Kanitpanyacharoen, V. Raju, P. Kaercher, J. Knight, A. McDowell, H.-R. Wenk, Q. Williams, and E. Zepeda, Rev. Sci. Instrum. **84**, 025118 (2013).
[26] L. Lutterotti, S. Matthies, H.-R. Wenk, A. S. Schultz, and J. W. Richardson, J. Appl. Phys. **81**, 594 (1997).
[27] J. Zhang *et al.*, J. Phys. Chem. Solids **66**, 1213 (2005).
[28] R. A. Lebensohn and C. N. Tome, Acta Metall. Mater. **41**, 2611 (1993).